12 Materials for Spin Electronics

J. M. D. Coey

Physics Department, Trinity College, Dublin 2, Ireland

Abstract. Materials which are currently used in spin electronic devices, and materials which may be useful in future are discussed. These include iron- cobalt- and nickel-based alloys for spin polarization and analysis, metallic and insulating antiferromagnets for exchange bias and oxides for tunnel barriers. The 3*d* alloys also serve as detection or sensor layers. Permanent magnet materials play a role in biasing some device structures. Novel materials are half-metallic oxides for all-oxide devices, and magnetic semiconductors which may allow the integration of spin electronics and optoelectronics.

12.1 Introduction

This chapter presents magnetic materials of interest for spin electronic devices. The focus is on crystal structure and intrinsic magnetic properties of the bulk materials, although it must be remembered that when incorporated into devices these materials frequently form part of a thin film stack with a layer thickness < 10 nm. The structure and magnetic properties of thin films can differ significantly from those of the bulk. To cite just two examples, the atomic magnetic moments in a free surface layer of a ferromagnetic film may be enhanced because of band narrowing, and surface anisotropy is present which is typically $\simeq 0.1$ mJ m^{-2} with the anisotropy direction normal to the film surface.

The properties that are exploited in spin electronic devices are of several kinds, but they relate mainly to the hysteresis curve and magnetic-field-dependent transport properties. Most semiconductors and semimetals are nonmagnetic; they exhibit the normal Hall effect, and the classical B^2 magnetoresistance due to the Lorentz force $-\mathrm{e}\boldsymbol{v}\times\boldsymbol{B}$ acting on the electrons. When the mean free path is long, as in single-crystal films of bismuth [1], film dimensions influence the magnetoresistive response. However, it is unnecessary to consider the spin of the electrons to explain these magnetoelectronic effects; conventional electronics has ignored the spin on the electron.

For ferromagnets, it is convenient to distinguish *intrinsic* magnetic properties, which are independent of microstructure or nanostructure in all but the thinnest films, from *extrinsic* properties which derive from the microstructure or nanostructure in an essential way. Besides the big three: Curie temperature T_C, spontaneous magnetization M_S, and magnetocrystalline anisotropy K_1, intrinsic properties include band structure, conductivity ratio α for $\uparrow$ and $\downarrow$ electrons, magnetostriction λ_S, anisotropic magnetoresistance (AMR) and colossal magneto-resistance (CMR). The main two extrinsic properties are remanence

M.J. Thornton and M. Ziese (Eds.): LNP 569, pp. 277–297, 2001.

M_r, and coercivity H_c, but there is also induced anisotropy K_u, granular and powder magnetoresistance (PMR), giant magnetoresistance (GMR), and tunneling magnetoresistance in planar tunnel junctions (TMR). GMR and TMR are at the heart of spin electronics, as we know it at present.

The magnetic materials principally used in spin electronics are soft ferromagnetic alloys of the late 3*d* metals. These serve as sources and conduction channels for the spin-polarized electrons, as well as magnetic flux paths and shields. Most progress has been made with sensors, ranging from simple position sensors and elements for nondestructive testing of ferrous metals to sophisticated miniature sensor elements in read heads for digital tape and disc recording where requirements are very demanding; high permeability is required with a sharp low-field switching response that extends to frequencies in the GHz range. Magnetic memory and logic elements require square hysteresis loops. All AMR, GMR, TMR and magnetic random access memory (MRAM) devices developed so far are based on 3*d* ferromagnetic metals and alloys. So too are magnetic three-terminal devices such as spin transistors and spin injection switches, as well as the magnetic Schottky barriers for injecting spin-polarised hot electrons into semiconductors.

Antiferromagnets, which may be metals or insulators, find a use in exchange biasing of magnetic thin film structures. Hard magnetic materials in thin film form can be employed to generate a stray field to stabilize a particular domain structure in a contiguous soft layer. Ferromagnetic oxides are at the research stage, but it is hoped that in future their half-metallic character will be exploited in sources and analysers of completely spin-polarized electrons. Magnetic semiconductors are another class of potentially-interesting materials, but they suffer from the critical defect that their Curie temperatures are far below room temperature.

Here, each of the main groups of actually or potentially useful materials will be presented, and some alloys of interest for particular applications are highlighted.

12.2 Iron Group Alloys

First we review the ferromagnetic elements Fe, Co and Ni, and then discuss alloy systems based on these three elements. Each has a different crystal structure, body-centred cubic (bcc) for iron, hexagonal close-packed (hcp) for cobalt and face-centred cubic (fcc) for nickel. Their electronic densities of states are compared in Fig. 12.1. All three transition elements have a broad, almost unpolarised *sp* band superposed on a spin-split 3*d* band. The unsplit density of states $D(E)$ exhibits a peak at the Fermi level E_F so that the Stoner criterion for spontaneous ferromagnetism $D(E_F)I > 1$ is satisfied. The exchange interaction I in the 3*d* band is $\simeq 1$ eV for all three ferromagnetic elements [2]. Iron, which has the largest atomic moment of 2.22 Bohr magnetons (μ_B), is a weak ferromagnet in the sense that there are both $3d\uparrow$ and $3d\downarrow$ electrons at the Fermi level. Cobalt and nickel, which have smaller moments, are strong ferromagnets in the sense that the $3d\uparrow$ states lie entirely below the Fermi level. The electronic configu-

ration of Ni, for example, is approximately $3d^{\uparrow 5.0}3d^{\downarrow 4.4}4s^{0.3}4p^{0.3}$, which gives a spin-only moment of $0.62\mu_{\mathrm{B}}$. Cobalt has an orbital moment of $\simeq 0.15\mu_{\mathrm{B}}$ and a total moment of $1.73\mu_{\mathrm{B}}$. The atomic moments quoted are at zero temperature.

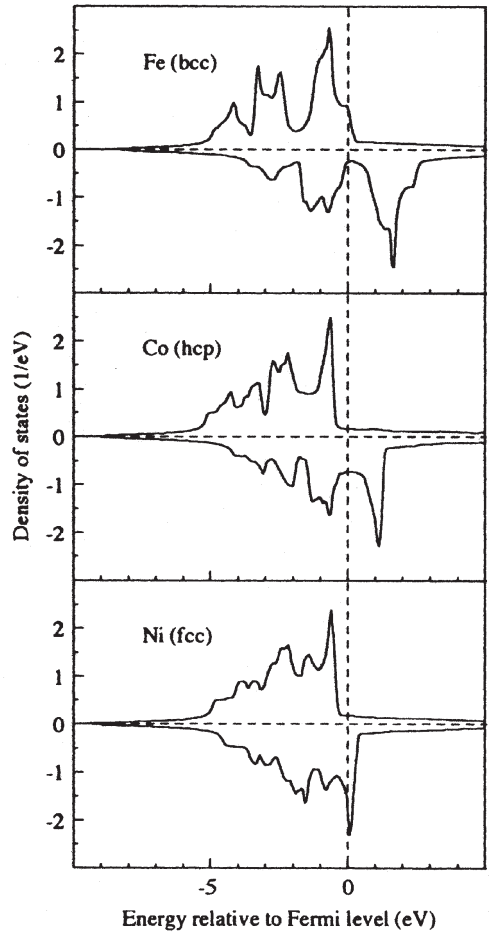

Fig. 12.1. The spin-split densities of states $D(E)$ calculated for iron, cobalt and nickel at zero temperature.

Strong ferromagnets were expected to show a higher value of spin polarization P of emitted electrons and a larger resistivity ratio α for $\uparrow$ and $\downarrow$ carriers than weak ferromagnets because scattering of sp electrons into the filled $3d\uparrow$ states is suppressed. In fact P turns out to be almost the same in magnitude and, more significantly of the same sign for all three ferromagnetic elements. P is easy to define, but difficult to measure. The definition is simply $(n^{\uparrow}-n^{\downarrow})/(n^{\uparrow}+n^{\downarrow})$ where $n^{\uparrow,\downarrow}$ is the number of conduction electrons of either spin in the unit cell, but in

any experiment to measure $n^{\uparrow,\downarrow}$ a weighting factor is involved which depends on how the spin-polarized electrons are detected [3]. Methods for measuring P include measuring the $I:V$ characteristic after applying a field to a tunnel junction between the ferromagnet and a thin film of superconducting aluminium, or measuring the $I:V$ characteristic of a point contact between a superconducting tip and the ferromagnet (Andreev reflection).

A summary of the main intrinsic properties of the ferromagnetic elements at room temperature is given in Table 12.1 [4]. Values refer to room temperature, except for the spin polarization, which was measured by Andreev reflection at 4.2 K [5].

Table 12.1. Intrinsic magnetic properties of Fe, Co and Ni.

	structure /density (kg m^{-3})	lattice parameters (pm)	T_C (K)	M_S (MA m^{-1})	K_1 (kJ m^{-3})	λ_S (10^{-6})	α	P (%)
Fe	bcc 7874	287	1044	1.71	48	−7	1.6	45
Co	hcp 8836	251 407(fcc)	1388	1.45	530	−62	8.0	42
Ni	fcc 8902	352	628	0.49	−5	−34		44

A number of derived properties important for aspects of nanoscale magnetism are listed in Table 12.2. These are the exchange stiffness A, the exchange length $l_{ex} = \sqrt{A/\mu_0 M_S^2}$ and the Bloch domain wall width $\delta_W = \sqrt{A/K_1}$. The coherence radius $l_{coh} = \sqrt{24} l_{ex}$, the single-domain particle size $d_{sd} = 72\sqrt{(AK_1)/\mu_0 M_S^2}$ and the superparamagnetic blocking diameter at room temperature $(150 k_B T/\pi K_1)^{1/3}$ refer respectively to the reversal mechanism, domain structure and stability of small particles. Analogous quantites can be defined for thin films. Other significant length scales are the mean free paths λ for $\uparrow$ and $\downarrow$ electrons and spin-diffusion length λ_{sd}; the spin diffusion length is usually one or two orders of magnitude greater than the mean free path, because spin-flip scattering events are comparatively rare. The mean free path is relevant for in-plane conduction in multilayer stacks, the usual GMR configuration. For cobalt, $\lambda^{\uparrow} \simeq 5.0$ nm, $\lambda^{\downarrow} \simeq 0.6$ nm. The spin diffusion length is the appropriate scale for perpendicular-to-plane conduction. λ_{sd} is about 50 nm for Co [6]. Some desirable properties sought in soft ferromagnetic $3d$ alloys are a high magnetization and high degree of spin polarization, low anisotropy and zero magnetostriction, since a stress σ induces a uniaxial anisotropy $K_{stress} = (3/2)\lambda_S \sigma$. Often it is desirable to create a weak uniaxial anisotropy K_u ($\simeq 1$ kJ m^{-3}) by processing a thin film of a disordered alloy in an applied magnetic field, which creates some slight texture or pair ordering on an atomic scale. The weak induced anisotropy increases

the permeability in the longitudinal direction, giving a square hysteresis loop with little coercivity. In the transverse direction there is a straight anhysteretic magnetization curve saturating at $2K_u/\mu_0 M_S$ (Fig. 12.2).

Table 12.2. Derived properties for Fe, Co and Ni.

	A (pJ m^{-1})	l_{ex} (nm)	δ_B (nm)	l_{coh} (nm)	d_{sd} (nm)	d_{sp} (nm)
Fe	8.3	1.5	41	7.4	12	16
Co	10.3	2.0	14	9.7	64	7
Ni	3.4	3.4	82	16	31	34

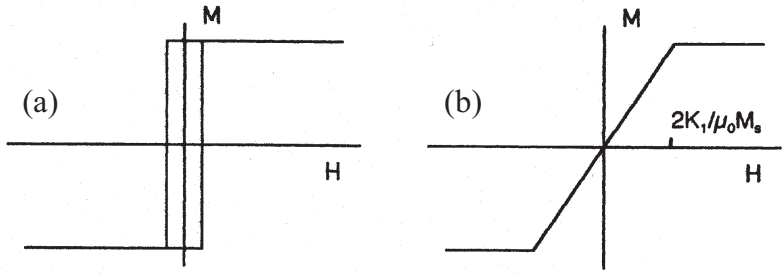

Fig. 12.2. Hysteresis loops for a soft magnetic material with weak induced uniaxial anisotropy, measured (a) in the longitudinal direction and (b) in the transverse direction.

Resistivity is also an issue in devices which switch at high frequency. Useful approaches are lamination of metallic and insulating films, or decorating grain boundaries to make them resistive, thereby minimizing eddy current losses. Amorphous alloys have the advantage of an intrinsically high resistivity, of order 1.5 $\mu\Omega$ m, which is the maximum possible for a homogeneous metal since the mean free path can be no shorter than the interatomic separation. The magnetocrystalline anisotropy of isotropic amorphous alloys is zero. As with disordered crystalline alloys, weak uniaxial anisotropy K_u can be induced by annealing or depositing the material in a uniform magnetic field.

A famous summary of the magnetic moment per atom in binary $3d$ alloys is the Slater–Pauling curve, shown in Fig. 12.3. The main branch, with slope -1 accounts for the strong ferromagnets having a filled $3d^{5\uparrow}$ subband. Each electron removed comes essentially from the $3d^{\downarrow}$ subband and increases the spin moment by $1\mu_B$. Extrapolating the curve to hypothetical strongly-ferromagnetic iron gives a moment of $2.6\mu_B$. The branches with slope $\simeq 1$ represent the moments of alloys between early and late transition metals, where the $3d$ states of the early transition elements lie well above the Fermi level of the late transition

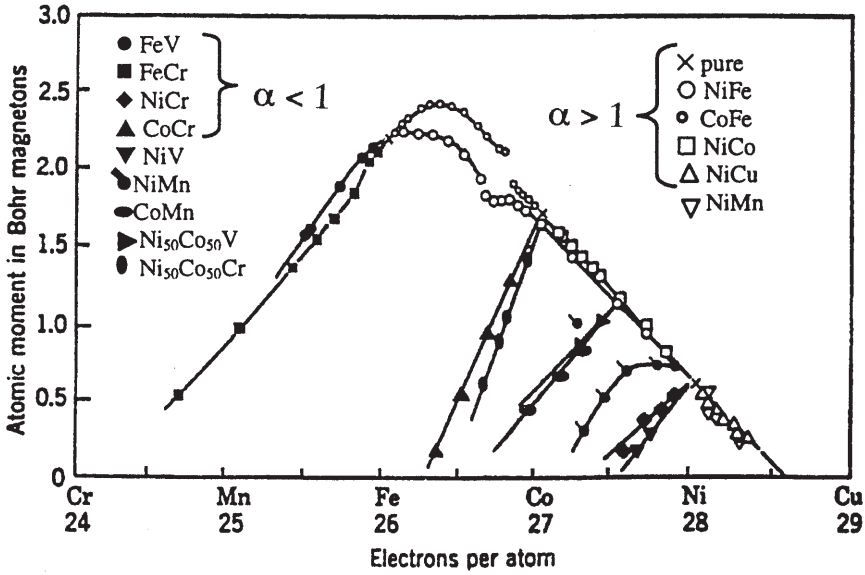

Fig. 12.3. The Slater–Pauling curve (after ref. [7]).

elements. The conductivity ratio $\alpha < 1$ for alloys on the branches with positive slope, whereas $\alpha > 1$ on the branch with negative slope [7]. Moments in strong ferromagnets are described quantitatively by the magnetic valence model [8], which is a generalization of these ideas. The chemical valence Z of an atom is $n^{\uparrow} + n^{\downarrow}$, where $n^{\uparrow,\downarrow}$ are the number of valence electrons with either spin. The spin moment in units of μ_{B} is $n^{\uparrow} - n^{\downarrow} = 2n^{\uparrow} - Z$. Now $n_d^{\uparrow}$ is precisely 5 for strong ferromagnets, so the magnetic valence defined by $Z_m = 2n_d^{\uparrow} - Z$ is an integer. The moment m is therefore $Z_m + 2n_{sp}^{\uparrow}$ where $n^{\uparrow} = n_d^{\uparrow} + n_{sp}^{\uparrow}$, and $2n_{sp}^{\uparrow}$ is the number of electrons in the *sp* band, which is practically unpolarized. In an alloy, the average moment *per atom* is deduced by replacing Z_m by its average over all the atoms present;

$$\langle m \rangle = \langle Z_m \rangle + 2n_{sp}^{\uparrow}\,. \tag{12.1}$$

Here $n_d^{\uparrow}$ is 5 for iron and atoms to the right, but zero for atoms at the beginning of the 3*d* series. Z_m is -3 for Sc, Y, B ...; -4 for Ti, Zr, C ..., 2 for Fe, 1 for Co and 0 for Ni. $2n_{sp}^{\uparrow}$ is about 0.3.

12.2.1 Iron–based Alloys

Besides the fact that it is not a strong ferromagnet, the problems with iron are its anisotropy and magnetostriction (Table 12.1). K_1 is fairly large for a cubic material, and λ_{S}, which is an isotropic polycrystalline average, is the resultant of bigger values in the $\langle 100 \rangle$ and $\langle 111 \rangle$ directions, 21×10^{-6} and -20×10^{-6}, respectively.

Alloying iron with cobalt produces a strong ferromagnet at $Fe_{65}Co_{35}$ (*Permendur*) which holds the record room-temperature magnetization of 1.95 MA m^{-1}, corresponding to a ferromagnetic polarization $\mu_0 M_S = 2.45$ T. The magnetization and Curie temperature are almost constant in Fe_xCo_{100-x} for $35 \leq x \leq 55$. The anisotropy of bcc Co is about -60 kJ m^{-3}, so zero anisotropy occurs at $x \simeq 55$. Unfortunately λ_S is 60×10^{-6} and the alloy usually has low permeability. The near-equiatomic compositions have a tendency to CsCl-type order (Fig. 12.4) and a unique axis may be induced by field annealing which can lead to $H_c \simeq 15$ A m^{-1} and an initial permeability $\mu_I \simeq 800$.

Generally it is not possible to find a composition in a binary alloy system where K_1 and λ_S go to zero simultaneously. By chance this almost happens in the Fe-Ni system (*Permalloy*) discussed below. A bcc iron-based ternary system which does have a $K_1 = 0$; $\lambda_S = 0$ point is Fe-Si-Al at the composition $Fe_{74}Si_{16}Al_{10}$ (*Sendust*). The alloy has a tendency to order in the Fe_3Si superstructure, and atomic order and composition must be accurately controlled to achieve optimum properties. Polarization is 1.2 T. Sendust has been used in write heads for magnetic recording.

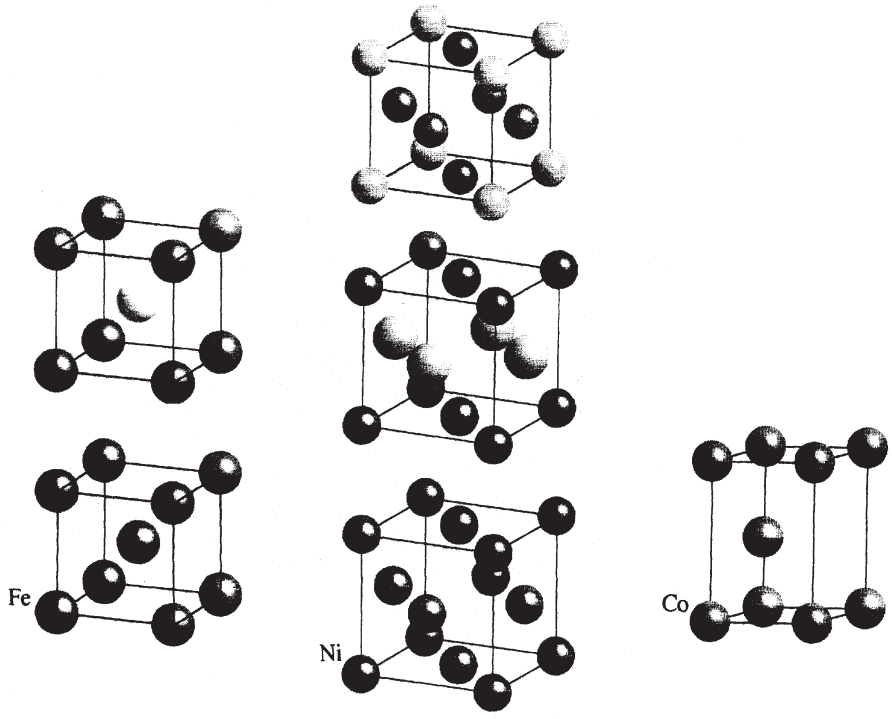

Fig. 12.4. Some simple crystal structures for metals; body-centred cubic (Fe) with the CsCl superstructure; face-centred cubic (Ni) with the $CuAu_3$ and tetragonal CuAu(I) superstructures; hexagonal close packed (Co).

Another approach is to prepare thin films with a concentration of dissolved nitrogen in excess of equilibrium by reactive sputtering. These have composition around $Fe_{97}N_3$ [9]. A few percent of an element such as Al, Ta, Ti or Rh serves to increase the solubility of nitrogen in iron or extend the stable α-phase field. The saturation magnetostriction changes sign at about 3% N, and the use of additions inhibits grain growth and thereby helps to stabilize soft magnetic properties by *anisotropy averaging*. In soft ferromagnetic nanostructures, the characteristic length scale for anisotropy averaging is the domain wall width which sets the scale for the smallest possible domain size

$$\delta_B = \pi\sqrt{A/K_1}\,. \tag{12.2}$$

The number of crystallites of average diameter D within a volume of δ_B^3 is $N = (\delta_B/D)^3$. Anisotropy directions of the crystallites are random, so the effective anisotropy constant is $\langle K\rangle \simeq K_1/\sqrt{N}$. Hence

$$\langle K\rangle \simeq K_1(D/\delta_B)^{3/2}\,. \tag{12.3}$$

But it is this effective anisotropy constant which must be used to determine the domain wall width. Substituting from (12.2) with K_1 replaced by $\langle K\rangle$ yields

$$\langle K\rangle \simeq K_1^4 D^6/\pi^6 A^3\,. \tag{12.4}$$

Taking $D = 20$ nm and the values for iron in Table 12.1 leads to $\langle K\rangle \simeq 0.6$ kJ m^{-3}, a reduction of the anisotropy by two orders of magnitude. Anisotropy averaging in soft exchange-coupled nanostructures is a powerful way of making them very soft indeed [10]. An example here is *Finemet*, a two-phase nanostructure of crystalline $Fe_{80}Si_{20}$ regions in an amorphous Fe-B matrix. The composition is $Fe_{73.5}Si_{15}B_{7.5}Cu_1Nb_3$. Copper and niobium additions serve to promote nucleation of the Fe-Si crystallites and refine the grain structure, respectively. The anisotropy of the Fe-Si crystallites is exchange-averaged to zero and the contributions to λ_S of the crystalline and amorphous regions are of opposite sign and cancel, yielding an iron-based nanocomposite with exceptionally high permeability. A variant on this is the Fe-Co-B system where nanometer-scale Fe-Co-rich regions are dispersed in a boron-rich amorphous matrix. A typical composition is $Fe_{62}Co_{21}B_{17}$, with polarization $\simeq 1.6$ T.

One other iron nitride that deserves a mention is the metastable α'-$Fe_{16}N_2$. It has been reported to have a moment in thin film form as high as $3.5\mu_B$/Fe [11], but this result have not been independently confirmed, and are at variance with theoretical expectations. Recent surveys of the literature on this material place its likely room-temperature polarization at 2.3(1) T [9,12]. However, it is claimed that imperfectly-ordered thin films ($\simeq 40$ nm) with a large cell volume have a moment of $2.8\mu_B$/Fe [13], corresponding to a polarization of 2.5 T. The tetragonal α' phase has a large uniaxial anisotropy of order 1 MJ m^{-3} [12], so anisotropy averaging here would need impracticably small crystallites, of diameter 2-3 nm.

12.2.2 Nickel–based Alloys

The fcc Ni_xFe_{100-x} system includes the famous *Permalloy* composition range $78 \leq x \leq 81$. Permalloy is probably the best-studied soft magnetic material, as it is very suitable for thin film devices. Permalloy is a strong ferromagnet with a polarization $\mu_0 M_S \simeq 1.0$ T. The conductivity ratio for $\uparrow$ and $\downarrow$ electrons is $\alpha = 6$ and the degree of spin polarization for emitted electrons is $P = 0.37$ [5]. The degree of ordering of Fe and Ni in the Cu_3Au structure (Fig. 12.4b) can be adjusted by heat treatment, and weak uniaxial anisotropy can be induced by field annealing. Cobalt is added to fcc Ni-Fe alloys around the permalloy composition range to increase their magnetization and improve their susceptibility to magnetic field treatment. It is then possible to induce the uniaxial anisotropy by depositing the film in an applied field of order 1 kA m^{-1}, which is preferable to field annealing for device structures as it avoids possible interdiffusion of the layers. In films thinner than 20 nm, the induced anisotropy K_u is proportional to film thickness. A typical composition is $Ni_{65}Fe_{15}Co_{20}$.

The particular feature of permalloy is that K_1 and λ_S change sign at nearly the same composition, making it possible to achieve an excellent soft magnetic response in a binary system (Fig. 12.5). Small additions of Mo or Cu are used to optimize the properties. Permalloy films have a good AMR response of 2% in a field of about 300 A m^{-1}. For this reason permalloy was used in AMR read heads. Thicker films ($\simeq 1$ μm) of permalloy are used in thin film write heads for hard discs and tapes. Produced by electrodeposition [14] from a single bath containing iron and nickel salts together with additives such as saccharine which serve to relieve the strain in the deposited film or increase its resistivity, these films are also employed for on-chip inductors. Uniaxial anisotropy is achieved by electrodeposition in a magnetic field of order 40 kA m^{-1}.

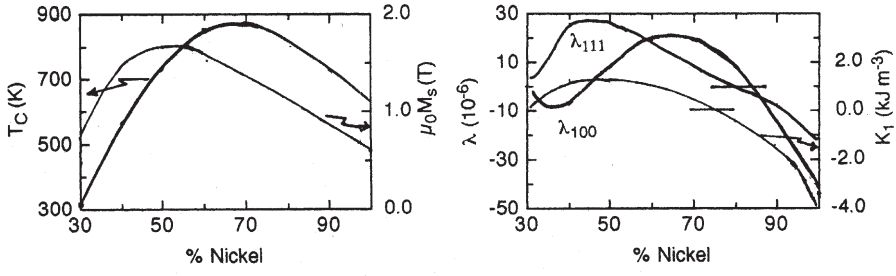

Fig. 12.5. Magnetic properties of Ni-Fe alloys.

The main drawback of permalloy is its relatively low polarization, which limits the field that can be generated and makes it unsuitable for ultrahigh-density write heads. The $Ni_{50}Fe_{50}$ composition is better in this respect, since $\mu_0 M_S = 1.6$ T. However the ultimate recording densities will need an excellent soft material with a polarization greater than 2.0 T, which cannot be achieved

in the Ni-Fe system. A third region of interest in the Ni-Fe series is Invar around $Ni_{35}Fe_{65}$, which is at the limit of the fcc phase field. Here T_C is low and the natural thermal expansion over a limited range of temperature around ambient is compensated by the temperature-dependent spontaneous volume magnetostriction ω_S, which is independent of applied field for a strong ferromagnet.

Anisotropy, but not magnetostriction can be suppressed by preparing Ni-Fe alloys in an amorphous form, using boron as a glass former. *Metglas 2628* a-$Fe_{40}Ni_{40}B_{20}$) is one such alloy. It has a random-dense-packed Bernal structure, with boron occupying the large intersticies in the random packing. The polarization, 0.8 T, is much reduced compared to $Ni_{50}Fe_{50}$ because of the presence of boron, which has a magnetic valence of −3, and the lower density of the amorphous dense-packed structure.

12.2.3 Cobalt–based Alloys

Cobalt normally has an hexagonal close-packed structure with a fairly large uniaxial anisotropy of $K_1 = 530$ kJ m^{-3}, corresponding to an anisotropy field $H_a = 2K_1/\mu_0 M_S$ of 0.57 MA m^{-1}. Cobalt can be easily stabilized in an fcc structure and the quoted Curie temperature, which is the highest known for any material, actually refers to the fcc phase. Cobalt is used in alloys to increase T_C. The atomic moment is unusually robust and structure independent. A thin (0.4 nm) fcc film at the interface between magnetic and nonmagnetic layers serves to provide a magnetically-sharp interface which promotes spin-dependent scattering [15]. Iron and boron are sometimes added to the interfacial cobalt. A typical composition is $Co_{87}Fe_9B_2$. Co-Fe-B is also used for the free layer of spin valves, where the additives allow enhanced uniaxial anisotropy and improve the thermal stability.

The anisotropy of hcp cobalt is insufficient to make a true permanent magnet, for which the anisotropy field $H_a = 2K_1/\mu_0 M_S$ would have to be significantly greater than the magnetization. Nevertheless, thin films with in-plane c-axis orientation can exhibit useful coercivity. Magnetization is in-plane in most magnetic thin film device structures and the demagnetizing field is small. Thin film media for hard discs are based on hexagonal cobalt with Cr, Pt and B additions which help create a layer of magnetically-decoupled Co-rich crystallites about 20 nm thick and 10-20 nm in size. Coercivity is $\simeq 300$ kA m^{-1}. A typical composition is $Co_{67}Cr_{20}Pt_{11}B_6$.

Cobalt-based alloys with a uniaxial crystal structure easily develop a very large anisotropy field and exhibit permanent magnet properties. A good example is YCo_5 where yttrium occupies alternate planes in the hexagonal structure. The anisotropy field $H_a = 12.3$ MA m^{-1}. Another structure with uniaxial anisotropy is the face-centred tetragonal CuAu(I) structure adopted by CoPt, and illustrated in Fig. 12.4b. Alternate planes are composed of Co and Pt, and the anisotropy field is 9.8 MA m^{-1}. The cubic $CuAu_3$ type of order occurs in $CoPt_3$, which is a semihard material that has been used in demonstration MRAM devices. Polycrystalline films of Co-Cr-Pt and CoPt with the c-axis in-

plane are used as permanent magnets to longitudinally bias and stabilize the domain structure in both AMR and GMR read heads.

Cobalt-based alloys with the fcc structure and amorphous cobalt-based alloys are much softer. In the Fe-Co-Ni system, nanocrystalline electrodeposited alloys at the border of the fcc and bcc phase fields have exchange-averaged anisotropy and near-zero magnetostriction. There are reports of polarization in excess of 2.0 T for $Co_{65}Ni_{12}Fe_{23}$ [16], $Co_{56}Ni_{13}Fe_{31}$ [17] and $Co_{52}Ni_{29}Fe_{19}$ [18]. Amorphous cobalt-rich alloys of composition $(CoFe)_{80}B_{20}$ can have zero magnetostriction, and are excellent high-permeability materials. The amorphous $Co_{90}Zr_{10}$ system also shows a zero magnetostriction point when a few percent of tantalum or rhenium is substituted for zirconium, or some nickel is substituted for cobalt. Polarization is about 1.4 T. The amorphous alloys are mechanically much harder than permalloy, and they are suitable for thin film write heads.

12.3 Antiferromagnets

It is common practice to pin the direction of magnetization of one of the ferromagnetic layers in a spin valve by exchange coupling to an antiferromagnet [19]. When the Curie temperature of the ferromagnet is greater than the Néel temperature of the antiferromagnet $T_C > T_N$ the direction of magnetization of the pinned layer may be set by cooling the exchange couple in a magnetic field. Otherwise it may be necessary to deposit or anneal the antiferromagnet in a large applied field. The direction of magnetization of the free layer in a spin valve can switch from antiparallel to parallel to the pinned layer under the influence of a small stray field which is sensed by the device (parallel anisotropies). Otherwise the direction of magnetization of the free layer may be set perpendicular to the direction of magnetization of the pinned layer with a small induced anisotropy K_u; the stray field then causes the magnetization of the free layer to rotate continuously (crossed anisotropies). These cases are illustrated schematically in Fig. 12.6.

Considering only the pinned layer of thickness t_p, its energy per unit area in the presence of an external field H is

$$E/A = -\mu_0 M_f H t_p \cos(\theta) + K_u t_p \sin^2(\theta) - \sigma \cos(\theta)\,, \tag{12.5}$$

where σ is the interface exchange coupling, which is of order 0.1 mJ m^{-2}. The origin of the exchange coupling at the interface is still a matter for discussion [19], but a common view is that the ferromagnetic and antiferromagnetic axes are perpendicular at the interface, and that a domain wall develops in the ferromagnetic layer, provided the antiferromagnetic layer exceeds the critical thickness t_0 needed to generate exchange bias. t_0 ranges from 7 nm for FeMn to 15 nm for a-$TbCo_3$ or > 50 nm for α-Fe_2O_3 [20].

The exchange coupling in (12.5) is represented by a field $H_{ex} = \sigma/\mu_0 M_p t_p$ acting on the pinned layer, which depends on temperature and falls to zero at a blocking temperature $T_b < T_N$. The unblocking of exchange bias can reflect a thermally-excited relaxation mode impeded by weak anisotropy, such as rotation

of the antiferromagnetic axis in the 111 plane of NiO, or else may reflect an atomic order-disorder transition. A typical room-temperature value of H_{ex} for a 5 nm thick pinned layer with $\mu_0 M = 1$ T is 20 kA m^{-1}. Some representative multilayer structures including an antiferromagnetic layer are shown in Fig. 12.7. In dual spin valves, the stacks are mirrored about a central free layer, which is sandwiched between two pinned layers. The quality of a spin valve depends on the field needed to switch the free layer, and the quantity $\Delta\rho/\rho = (\rho^{\uparrow\downarrow} - \rho^{\uparrow\uparrow})/\rho^{\uparrow\uparrow}$ where the double superscripts refer to the antiparallel or parallel configurations for the pinned and free layers. In a simple two-current model, this is related to α, the conductivity ratio for $\uparrow$ and $\downarrow$ electrons in the spin valve structure by the formula $\Delta\rho/\rho = (1 - \alpha^2)/4\alpha$ [20].

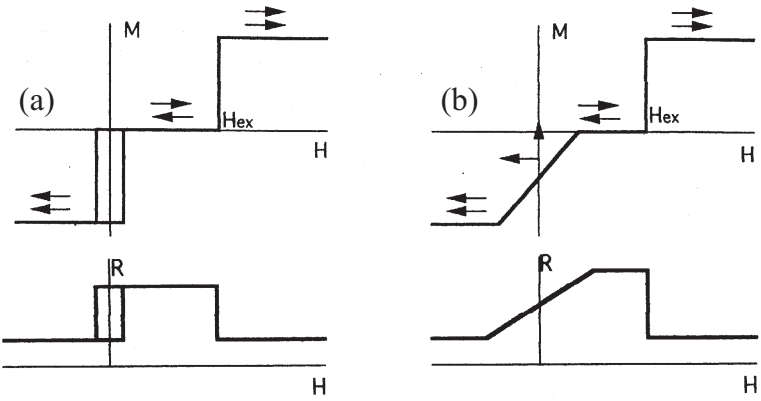

Fig. 12.6. Schematic response of a spin valve structure with (a) parallel and (b) crossed anisotropies.

Most of the antiferromagnets of interest for spin electronic devices are manganese alloys, whose properties are summarized in Table 12.3. Some oxides and amorphous materials are also useful. Manganese antiferromagnets close to the equiatomic composition may have a disordered fcc structure, or else adopt the face-centred tetragonal CuAu(I) structure illustrated in Fig. 12.4. The manganese alloys exhibit a great variety of collinear and noncollinear antiferromagnetic structures, yet all are able to provide exchange bias. For example, FeMn, which has been widely studied with permalloy as the adjacent ferromagnetic layer, has a disordered fcc crystal structure, and a magnetic structure with four sublattices oriented along the four $\langle 111 \rangle$ directions [4]. NiMn has a higher blocking temperature, and is chemically more inert than FeMn. It has the fct structure, and a magnetic structure of antiferromagnetic 002 planes, with $\boldsymbol{S} \parallel \boldsymbol{a}$. The quest for a high blocking temperature and the ability to conveniently set the antiferromagnetic axis has led to investigation of Ir-Mn, Rh-Mn and Pt-Mn alloys as well as pseudobinaries such as $(Pd_{1-x}Pt_x)Mn$ and Cr-Mn alloys. The bulk magnetic

Table 12.3. Antiferromagnetic materials for exchange bias [19,20,21]. $\boldsymbol{S}$ denotes the spin direction. $^{\#}$Order-disorder transition. *Sperimagnetic; T_{N} is the Néel temperature, T_{b} an irreversible transition.

		T_{N} (K)	T_{b} (K)	σ (mJ m^{-2})
FeMn	fcc; four noncollinear sublattices; $\boldsymbol{S} \parallel 111$	510	440	0.10
NiMn	fct; antiferromagnetic 002 planes, $\boldsymbol{S} \parallel \boldsymbol{a}$	$1050^{\#}$	700	0.27
PtMn	fct; antiferromagnetic 002 planes, $\boldsymbol{S} \parallel \boldsymbol{c}$	975	500	0.30
$RhMn_3$	triangular spin structure	850	520	0.19
$Ir_{20}Mn_{80}$	fct; parallel spins in 002 planes, $\boldsymbol{S} \parallel \boldsymbol{c}$	690	540	0.19
$Pd_{52}Pt_{18}Mn_{50}$	fct; antiferromagnetic 002 planes	870	580	0.17
a-$Tb_{25}Co_{75}$ *	$T_{\mathrm{comp}} = 340$ K	600	> 520	0.33
NiO	parallel spins in 111 planes, $\boldsymbol{S} \perp \langle 111 \rangle$	525	460	0.05
α-Fe_2O_3	canted antiferromagnet, $\boldsymbol{S} \perp \boldsymbol{c}$	950		

structures of the antiferromagnets summarized in Table 12.3 are not necessarily those of the thin films used for exchange bias.

It is important that the processing conditions needed for the magnetic material are compatible with the other materials present in the device. If, for example, magnetic devices such as MRAM are to be integrated with silicon electronics, the exchange couple should be stable at temperatures used in silicon processing, typically $> 300°$C for one hour to reduce radiation damage, and 200°C for up to six hours for packaging. $Ir_{20}Mn_{80}$ might be suitable in this respect [22,23].

Some antiferromagnetic oxides are also useful. NiO has the highest Néel temperature of the monoxides, but T_{b} is rather low; the anisotropy can be enhanced by cobalt substitution. Nevertheless NiO has been used in commercial spin-valves. α-Fe_2O_3 has a high Néel temperature, but a thick layer is needed because of the low anisotropy of the antiferromagnet due to the proximity to room temperature of the Morin transition, where the antiferromagnetic anisotropy constant K_1 changes sign. The orthoferrites $RFeO_3$, which have T_{N} in the range 620-740 K, are also being investigated. Oxides have the bonus that they act as specularly reflecting layers, which enhance the efficiency of spin valve structures.

A more recent development is the *artificial antiferromagnet* (AAF) [24] (Fig. 12.7). This is a stack of two or more ferromagnetic layers separated by layers of a nonmagnetic metal whose thickness is chosen to provide an antiferromagnetic interlayer exchange. Best is cobalt separated by a very thin layer,

$\simeq 0.6$ nm, of ruthenium. Iron or iron and boron additions facilitate the creation of induced anisotropy in the cobalt. Copper can be used as a weaker coupling layer [25]. The upper cobalt layer of the AAF can serve as the pinned layer of the spin valve, and layer thicknesses adjusted to give no stray field on the free layer. One of the exchange bias antiferromagnets just discussed can then be used to pin the lower cobalt layer, (Fig. 12.7). Annealing in a rather large field ($\simeq$ 1 MA m^{-1}) is needed to saturate the AAF and fix the antiferromagnetic axis, but spin valves with an AAF pinned layer (Fig. 12.7) show better thermal stability and larger exchange bias than the basic configuration (Fig. 12.7) [26,27]. Stacks for dual spin valves with artificial antiferromagnets become impressively complex, with up to 15 layers [28] composed of as many as seven different materials, four of which are magnetic (AF bias layer, AAF magnetic layers, free layer, interface layer).

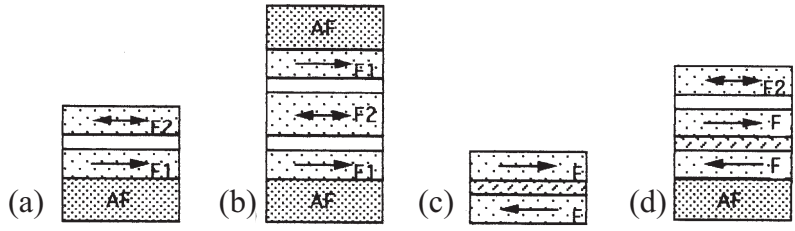

Fig. 12.7. Magnetic multilayers: (a) simple spin valve with an antiferromagnetic pinning layer, (b) double spin valve (c) an artificial antiferromagnet, (d) a spin valve based on an artificial antiferromagnet. The interfaces between the magnetic layers (F1, F2) and the spacer layer (unshaded) are often decorated with an ultrathin cobalt layer to improve $\Delta\rho/\rho$ for the devices.

12.4 Oxides and Half–metals

Thin oxide layers, usually 1-2 nm of nanocrystalline Al_2O_3, are used as barrier layers in planar tunnel junctions. These current-perpendicular-to-plane devices have at least twice the sensitivity ($\Delta\rho/\rho$) of GMR spin valves. Their high intrinsic resistance and low power consumption makes them attractive for applications such as MRAM [29]. For read heads, a lower resistance is required, and the oxide barrier must then be very thin [30]. The most popular method for producing the Al_2O_3 barrier layer is by plasma oxidation of a layer of aluminum metal. Thermal oxidation in air is also used, but the best resistivities, of order 1 kΩ μm^2, may be obtained by oxidation assisted by ultraviolet light [31]. Other barrier oxides which have been investigated include $SrTiO_3$, TiO_2 and CeO_2. The magnetoresistive response of the tunnel junction depends on the nature of the barrier layer [32]. The ferromagnetic electrodes in almost all the devices showing a useful effect at room temperature have been the 3d alloys discussed in Sect. 12.2.

Ferromagnetic metallic oxides and related compounds can act as sources and conduction channels for the spin-polarized electrons. The 3*d* metals, even those that are strong ferromagnets, suffer from incomplete spin polarization of the conduction electrons because of the presence of the $4s/4p$ bands, which are not spin-split. In principle, a more favourable situation can arise in oxides where hybridization of the outer metallic electron shells with the $2p$(O) orbitals produces a gap of several eV between them. The 3*d* bands and the Fermi level tend to fall in this *s*-*p* gap. When the Fermi level intersects only one of the spin-polarized 3*d* bands, and there is a gap in the density of states for the other spin direction we have a half-metallic ferromagnet (Fig. 12.8). A feature of a stoichiometric half-metallic ferromagnet is that the spin moment should be an integral number of Bohr magnetons. This follows since $n^{\uparrow} + n^{\downarrow}$ is an integer in a stoichiometric compound and $n^{\downarrow}$ is an integer on account of the gap. Hence $n^{\uparrow} - n^{\downarrow}$ is an integer.

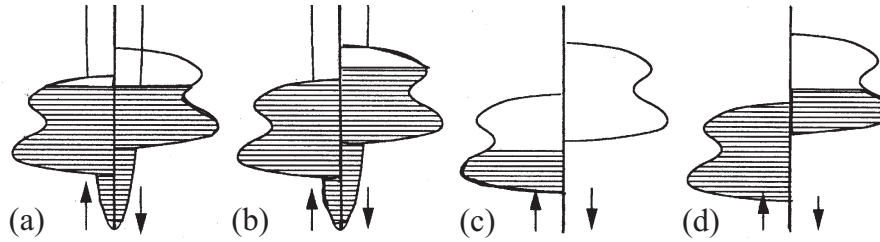

Fig. 12.8. Schematic densities of states for (a) a weak ferromagnet, (b) a strong ferromagnet and (c) and (d) half-metallic ferromagnets where a gap arises for minority or majority-spin electrons.

Other compounds containing a main group element such as Sb, Si which hybridizes with the outer metallic orbitals can also have half-metallic character. Examples are the Heusler alloys NiMnSb, PtMnSb and Co_2MnSi. These alloys

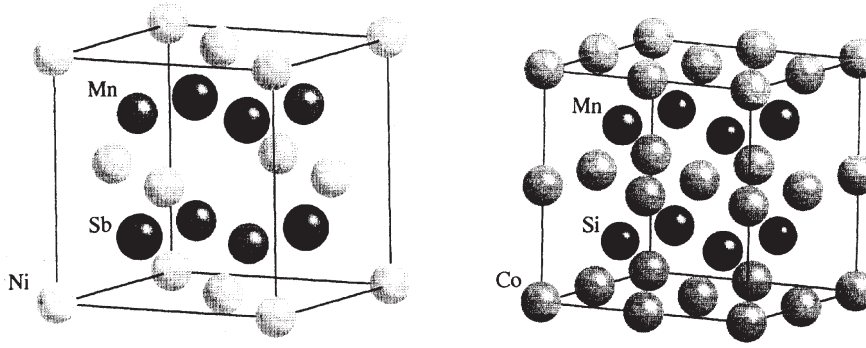

Fig. 12.9. Crystal structures of the Heusler alloys NiMnSb and Co_2MnSi.

have an ordered fcc structure, with the atoms ordered on three or four of the simple cubic sublattices (Fig. 12.9). Curie temperatures are 728, 572 and 985 K. Tunnel junctions have been built using NiMnSb [33]. Data on some half-metals is collected in Table 12.4.

We now consider a few oxides in turn. The first is CrO_2 which has the distinction of being the only simple oxide that is a ferromagnetic metal. The rutile structure is illustrated in Fig. 12.10. There the Cr^{4+} ion is surrounded by a nearly-undistorted oxygen octahedron. The primary effect of the crystal field due to the six oxygen anions is to split the $3d$ orbitals into a t_{2g} triplet (xy, yz, zx) and an e_g doublet (x^2-y^2, $3z^2$-r^2), with a crystal-field splitting of about 1.5 eV. (Fig. 12.10) The $3d$ orbitals overlap to form bands; the overlap of the xy orbitals in the rutile structure is slight, so they form an occupied nonbonding level with a localized $S = 1/2$ core spin. The other t_{2g} orbitals mix to form a broader half-filled band with a dip in $D(E)$ at E_F. The exchange mechanism in CrO_2 is a combination of ferromagnetic superexchange together with double exchange due to hopping of the band electrons from site to site, where they are coupled to the $S = 1/2$ cores by the on-site Hund's rule exchange. CrO_2 is a black metal with a low resistivity ($\simeq 0.05$ μΩ m) in the liquid helium range. There the mean free path is long enough for a classical B^2 magnetoresistance to be observed [34]. However, ρ increases rapidly as T approaches the Curie point $T_C = 398$ K, and the mean free path is reduced to the scale of the interatomic spacing by strong spin-flip scattering.

Table 12.4. Half-metallic ferromagnets.

	Structure	Lattice parameter (pm)	T_C (K)	m_0 (μ_B/ formula)	M_S (MA m^{-1})
NiMbSb	Cubic	592	728	4.0	0.71
CrO_2	Tetragonal	442; 292	398	2.0	0.40
$(La_{0.7}Sr_{0.3})MnO_3$	Rhombohedral	548; 60.4°	380	3.6	0.31
Sr_2FeMoO_6	Tetragonal	557; 791	426	3.5	0.15

Other metallic ferromagnetic oxide systems where the double exchange mechanism is important are the mixed-valence manganites $(La_{1-x}A_x)MnO_3$; A = Ca, Sr or Ba, $x \simeq 0.3$ [35]. These oxides exhibit a metal-insulator transition at the Curie point, which reaches a maximum value of 380 K in $(La_{0.7}Sr_{0.3})MnO_3$. This is accompanied by colossal magnetoresistance, an intrinsic effect associated with a field-induced increase of spontaneous magnetization near T_C. The oxides have the perovskite structure, and the electronic structure is shown schematically in Fig. 12.11. The half-filled e_g band associated with Mn^{3+} is split in $LaMnO_3$ by the Jahn-Teller effect. The band splitting is sufficient to make the end-member a narrow-gap antiferromagnetic semiconductor. Doping with A^{2+} introduces holes

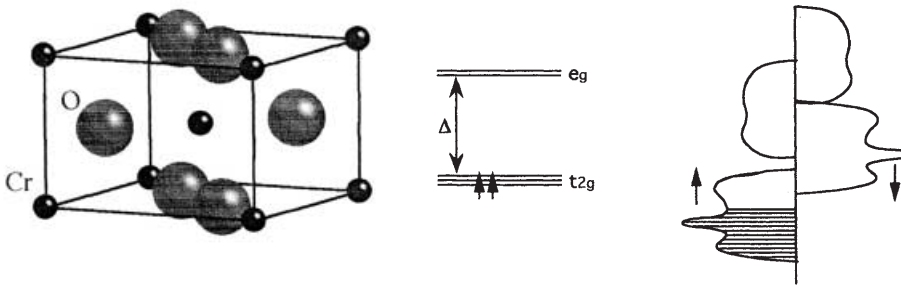

Fig. 12.10. Crystal structure of CrO_2. The effect of the crystal field on the one-electron $3d$ levels is shown, together with a schematic density of states.

into the lower spin-split e_g band, and when these are sufficiently numerous, the holes can move freely among the ferromagnetically-aligned t_{2g}^3, $S = 3/2$ cores. Hopping between the core spins provides the double exchange. If the cores are misaligned by an angle Ψ, the hopping probability varies as $\cos(\Psi/2)$. Electron transport is therefore inhibited in the magnetically disordered state above T_C, where the carriers are polarons of some description.

Magnetite, Fe_3O_4, is a ferrimagnet crystallizing in the spinel structure with a single $3d^{\downarrow}$ electron hopping among the $3d^{5\uparrow}$ cores on octahedral sites. This corresponds to a half-metallic density of states, but there is a strong tendency to form polarons below the Curie temperature (860 K), and the conductivity shows a small activation energy.

The magnetoresistance effects of most interest in the manganites, Fe_3O_4 and CrO_2 are associated with transport of spin polarized electrons from one ferromagnetic region to another with a different direction of magnetization. These regions are not usually separated by a domain wall, but by a grain boundary, an interparticle contact or planar tunnel barrier which does not transmit exchange coupling. The effects are seen in low fields and in the liquid helium tempera-

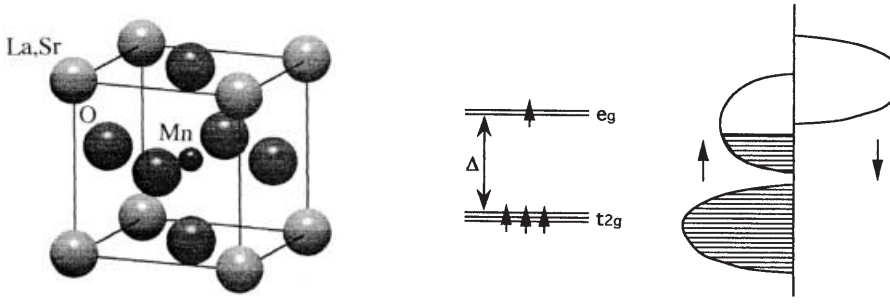

Fig. 12.11. Crystal structure of $(La_{0.7}Sr_{0.3})MnO_3$. The effect of the crystal field on the one-electron $3d$ levels is shown, together with a schematic density of states.

ture range they can reach 50% in CrO_2 pressed powder compacts, and several hundred % in planar manganite tunnel junctions [35]. Small effects have been observed in CrO_2 tunnel junctions [36,37]. The MR effects fall away fast on increasing temperature because of spin depolarization of the emitted electrons. Prospects of using CrO_2 or mixed-valence manganites in devices are dim, at least in a typical temperature range of −40 to 120°C. Progress with oxide spin electronics will require half-metallic compounds with higher Curie temperatures.

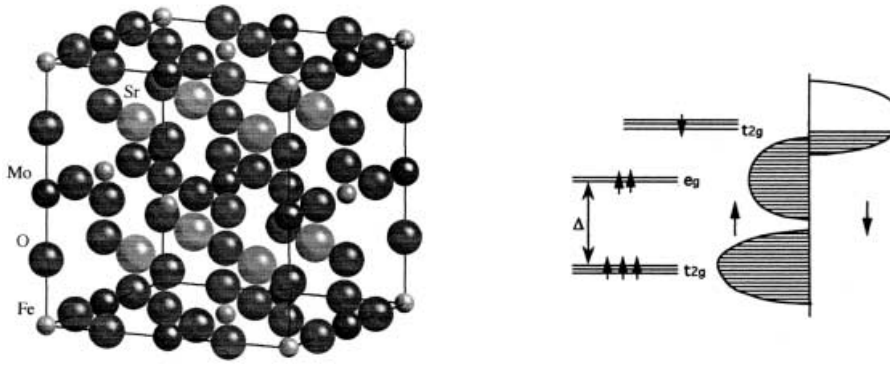

Fig. 12.12. Crystal structure of Sr_2FeMoO_6. The effect of the crystal field on the one-electron levels is shown, together with a schematic density of states.

Attention has recently turned to double perovskites with general formula $A_2BB'O_6$ where the B and B' cations occupy an NaCl-type superlattice (Fig. 12.12). The compound Sr_2FeMoO_6, for example, has a Curie temperature of 421 K and electronic structure calculations [38] indicate a half-metallic structure of the type shown in Fig. 12.6d. The majority spins are associated with the Fe^{3+}, $3d^5$ core spins, and the minority carriers are in a ↓ band of mainly $4d^1$(Mo) character which is mixed with the empty iron t_{2g} ↓ orbitals. The ferromagnetic exchange is due to this electron hopping among the $3d^{5\uparrow}$ cores. There is no Fe-O-Fe superexchange on account of the NaCl-type order of Fe and Mo. Quite a large granular magneto-resistance has been reported at room temperature [39]. Other double perovskites such as Sr_2FeReO_6 have been reported to have a substantially higher Curie temperature (540 K).

Compared to the metallic multilayer structures which have undergone very rapid development in the ten years or so since the discovery of GMR, mainly in response to the urgent demands of the magnetic recording industry, research on optimizing oxide structures is in its infancy. Much has to be done to understand and prevent spin depolarization at the interfaces, and there is scope for new materials development focussing on increasing the Curie temperature. The oxides offer the prospect of very large magnetoresistance effects which could eliminate the need for associated electronics in MRAM, as well as providing streams of spin-polarized electrons which can advance the science of spin electronics in the

21st century. The oxides are robust and may lead to low cost sensors for a range of mass-market applications.

12.5 Ferromagnetic Semiconductors

Integration of spin electronics with conventional electronics would entail the manipulation of spin-polarized currents in silicon or gallium arsenide (see chapter 17 for further details on ferromagnetic semiconductors). There is evidence that the spin diffusion length in these semiconductors is long, with values of many microns being reported for Si or GaAs. The difficulty has been to find an effective way of injecting the spin-polarized electrons.

A fully-dopable ferromagnetic semiconductor would be a formidable advance for spin electronics. Some ferromagnetic semiconductors do exist [40], including EuX; X=O, S, B_6, and the chalcogenide spinels $CdCr_2X_4$; X = S, Se. The MCr_2S_4 spinels with M = Mn, Fe, Co are ferrimagnetic semiconductors. Mn-doped GaAs is a tetrahedrally bonded material which has been successfully used for spin injection into GaAs [41], opening the prospect of a marriage of spin electronics and opto-electronics. The outstanding problem with all this that the Curie temperatures of all these ferromagnetic semiconductors is far below room temperature. It is predicted that Mn-doped GaN or ZnO should have Curie temperatures in excess of 300 K [42]. If this is true, a new chapter in spin electronics may open.

Problems

1. Use the magnetic valence model with $2n_{sp}^{\uparrow} = 0.6$ to deduce m_0, the magnetic moment in μ_B/formula unit, for the following alloys: $Ni_{65}Fe_{15}Co_{20}$, $Fe_{40}Ni_{40}B_{20}$ and $Co_{88}Zr_8Ta_4$. Give the corresponding values of the polarization $\mu_0 M_S$ in tests assuming the first two alloys are fcc with a packing fraction of 0.74, and the 3*d* transition elements in the second two alloys are random close-packed with a packing fraction of 0.64. Why are your values of polarization overestimated?
2. How small would the cobalt crystallites have to be if a polycrystalline film of hcp cobalt was to have an effective anisotropy constant of 1 kJ m^{-3}? Explain why alloy additions are used to decouple the cobalt crystallites in thin film magnetic media.
3. Use (12.5) to deduce the values of the external magnetic field which must be applied along the anisotropy axis to switch the magnetization of a pinned layer. Evaluate these fields for the case of a 10 nm layer of permalloy pinned by NiMn if $K_u = 500$ J m^{-3}. Estimate how big a field would be needed to obtain a symmetric hysteresis loop.
4. From the value of the magnetic moment M_0 for Sr_2FeMoO_6 given in Table 12.4, deduce the fraction of Fe and Mo atoms that are on the wrong sites in the NaCl-type superlattice. Justify the assumptions you make regarding the directions of magnetization of the misplaced atoms.

5. You are looking for a new ferromagnetic material to be used as a source of polarized electrons for spin electronics. Make a list of properties, in order of importance, that it should possess.

The Bibliography

R. C. O'Handley, "Modern Magnetic Materials", Wiley-Interscience, New York 1999, 740 pp.
U. Hartmann (ed.) "Magnetic Multilayers and Giant Magnetoresistance", Springer, Berlin 1999, 321 pp.
E. du Trémolet de Lacheisserie (ed.) "Magnétisme", 2 vols., Presses Universitaires de Grenoble 1999, 1006 pp.

References

1. F. Y. Yang, K. Liu, C. L. Chien, and P. C. Searson, Phys. Rev. Lett. **82**, 3328 (1999).
2. E. P. Wohlfarth in "Handbook of Ferromagnetic Materials" (E. P. Wohlfarth, ed.) vol. 1 North Holland, Amsterdam p.1 (1980).
3. I. I. Mazin, Phys. Rev. Lett. **83**, 1427 (1999).
4. "Magnetic Properties of Metals" , H. P. Wijn (ed.) Springer, Berlin 1991.
5. R. J. Soulen, J. M. Byers, M. S. Osofsky, B. Nadgorny, T. Ambrose, S. F. Chong, P. R. Broussard, C. T. Tanaka, J. S. Moodera, A. Barry, and J. M. D. Coey, Science **282**, 88 (1998).
6. A. Fert and L. Piraux, J. Magn. Magn. Mater. **200**, 338 (1999).
7. A. Barthélémy, A. Fert, and F. Petroff in "Handbook of Ferromagnetic Materials" (K. H. J. Buschow, ed.) vol. 12 North Holland, Amsterdam p.1 (1999).
8. A. R Williams, V. L. Moruzzi, A. P. Malozemoff, and K. Tekura, IEEE Trans. Magn. **19**, 1983 (1983).
9. J. M. D. Coey and P. A. I. Smith, J. Magn. Magn. Mater. **200**, 405 (1999).
10. G. Herzer in "Handbook of Ferromagnetic Materials" (K. H. J. Buschow, ed.) vol 10, North Holland, Amsterdam p.415 (1997).
11. Y. Sugita, M. Mitsuoka, M. Komuta, H. Hoshiya, Y. Kozono, and M. Hanazono, J. Appl. Phys. **79** 5576 (1996); H. Takahashi, M. Igarishi, A. Kaneko, H. Miyajima, and Y. Sugita, IEEE Trans. Magn. **35**, 794 (1999).
12. M. Takahashi and H. Shoji, J. Magn. Magn. Mater. **208**, 145 (2000).
13. S. Okamoto, O. Kitakami, and Y. Shimada, J. Magn. Magn. Mater. **208**, 102 (2000).
14. P. C. Andricarcos and N. Robertson, IBM J. Res. Dev. **42**, 671 (1998).
15. S. S. P. Parkin, Appl. Phys. Lett. **61**, 1358 (1992).
16. T. Osaka, M. Takai, K. Hayashi, Y. Sogawa, K. Ohashi, Y. Yasue, M. Saito, and K. Yamada, IEEE Trans. Magn. **34**, 1432 (1998).
17. T. Yokoshima, M. Kaseda, M. Yamada, T. Nakanishi, T. Momma, and T. Osaka, IEEE Trans. Magn. **35**, 2499 (1999).
18. X. Liu, G. Zangari and L. Shen, J. Appl. Phys. **87**, 5410 (2000).
19. A. E. Berkowitz and R. Takano, J. Magn. Magn. Mater. **200**, 552 (1999).
20. R. Coehoorn in "Magnetic Multilayers and Giant Magnetoresistance", (U. Hartmann, ed.) Springer, Berlin 1999, p 65.

21. M. Ledermann, IEEE Trans. Magn. **35**, 794 (1999).
22. D. Wang, M. Tondra, C. Nordman, and J. M. Daughton, IEEE Trans. Magn. **35**, 2886 (1999).
23. S. Tehrani, J. M. Slaughter, E. Chen, M. Durlam, J. Shi, and M. de Herrera, IEEE Trans. Magn. **35**, 2814 (1999).
24. H. A. M. van den Berg in "Magnetic Multilayers and Giant Magnetoresistance", (U. Hartmann, ed.) Springer, Berlin 1999, p 179.
25. H. A. M. van den Berg, J. Altman, L. Bär, G. Gieres, R. Kinder, R. Rupp, M. Veith, and J. Wecker, IEEE Trans. Magn. **35**, 2892 (1999).
26. H. Nagai, M. Ueno, F. Hikami, T. Sawasaki, and S. Tanoue, IEEE Trans. Magn. **35**, 2964 (1999).
27. Y. Sugita, Y. Kawawake, M. Satomi, and H. Sakakima, IEEE Trans. Magn. **35** 2961, (1999).
28. H. C. Tong, X. Shi, F. Liu, C. Qian, Z. W. Dong, X. Yan, R. Barr, L. Miloslavsky, S. Zhou, J. Perlas, S. Prabhu, M. Mao, S. Funada, M. Gibbons, Q. Leng, J. G. Zhu, and S. Dey, IEEE Trans. Magn. **35**, 2574 (1999).
29. J. M. Daughton, J. Appl. Phys. **81**, 3758 (1997).
30. R. Coehoorn, S. R. Cumpson, J. J. M. Ruijrok, and P. Hidding, IEEE Trans. Magn. **35**, 2586 (1999).
31. P. Rottländer, H. Kohlstedt, H. A. M. de Gronckel, E. Girgis, J. Schelten, and P. Grünberg, J. Magn. Magn. Mater. **210**, 251 (2000).
32. J. M. de Teresa, A. Barthélémy, A. Fert, J. P. Contour, F. Montaigne, and P. Seneor, Science **286**, 507 (1999).
33. C. T. Tanaka, J. Nowak, and J.S. Moodera, J. Appl. Phys. **86**, 6239 (1999).
34. S. M. Watts, S. Wirth, S. von Molnár, A. Barry, and J. M. D. Coey, Phys. Rev. B **61**, 149621 (2000).
35. J. M. D. Coey, M. Viret, and S. von Molnár, Adv. Phys. **48** 167 (1999).
36. A. Barry, J. M. D. Coey, and M. Viret, J. Phys.: Condens. Matter **12**, L173 (2000).
37. A. Gupta, X.W. Li, and Gang Xiao, J. Appl. Phys. **87**, 6073 (2000).
38. K. I. Kobayashi, T. Kimura, H. Sawada, K. Tekura, and Y. Tokura, Nature **385**, 677 (1998).
39. R. P. Borges, R. M. Thomas, C. Cullinan, J. M. D. Coey, R. Suryanarayanan, L. Ben-Dor, L. Pinsard-Gaudet, and A. Revcolevschi, J. Phys.: Condens. Matter **11**, L445 (1999).
40. S. Methfessel and D.C. Mattis, "Handbuch der Physik", **18** (Springer, Berlin 1966) p389.
41. Y. Ohno, D.K. Young, B. Beschoten, F. Matsukura, H. Ohno, and D. D. Awschalom, Nature **402**, 790 (1999).
42. T. Dietl, H. Ohno, F. Matsukura, J. Cibert, and D. Ferrand, Science **287**, 1019 (2000).